

## Immobilization of the Influenza A M2 Transmembrane Peptide in Virus Envelope—Mimetic Lipid Membranes: A Solid-State NMR Investigation<sup>†</sup>

Wenbin Luo, Sarah D. Cady, and Mei Hong\*

Department of Chemistry, Iowa State University, Ames, Iowa 50011

Received April 26, 2009; Revised Manuscript Received June 1, 2009

**ABSTRACT:** The dynamic and structural properties of membrane proteins are intimately affected by the lipid bilayer. One property of membrane proteins is uniaxial rotational diffusion, which depends on the membrane viscosity and thickness. This rotational diffusion is readily manifested in solid-state NMR spectra as characteristic line shapes and temperature-dependent line narrowing or broadening. We show here that this whole-body uniaxial diffusion is suppressed in lipid bilayers mimicking the composition of eukaryotic cell membranes, which are rich in cholesterol and sphingomyelin. We demonstrate this membrane-induced immobilization on the transmembrane peptide of the influenza A M2 (AM2-TM) proton channel protein. At physiological temperature, AM2-TM undergoes uniaxial diffusion faster than  $\sim 10^5 \text{ s}^{-1}$  in DLPC, DMPC, and POPC bilayers, but the motion is slowed by 2 orders of magnitude, to  $< 10^3 \text{ s}^{-1}$ , in a cholesterol-rich virus envelope—mimetic membrane (“viral membrane”). The immobilization is manifested as near rigid-limit  $^2\text{H}$  quadrupolar couplings and  $^{13}\text{C}-^1\text{H}$ ,  $^{15}\text{N}-^1\text{H}$ , and  $^{13}\text{C}-^{15}\text{N}$  dipolar couplings for all labeled residues. The immobilization suppresses intermediate time scale broadening of the NMR spectra, thus allowing high-sensitivity and high-resolution spectra to be measured at physiological temperature. The conformation of the protein in the viral membrane is more homogeneous than in model PC membranes, as evidenced by the narrow  $^{15}\text{N}$  lines. The immobilization of the M2 helical bundle by the membrane composition change indicates the importance of studying membrane proteins in environments as native as possible. It also suggests that eukaryote—mimetic lipid membranes may greatly facilitate structure determination of membrane proteins by solid-state NMR.

Lipid bilayers are now recognized to have significant impacts on membrane protein structure and dynamics. The thickness, fluidity, and charge of lipid membranes can modulate the orientation, dynamics, oligomeric state, and function of membrane proteins (1, 2). In particular, fluid bilayers endow membrane proteins with abundant dynamics that include both internal segmental motions and whole-body rotational and translational diffusions (3–5) from picoseconds to milliseconds. These motions usually have functional importance, such as facilitating large conformational changes (6), ion channel formation (7), and membrane disruption (8, 9).

The rate of large-amplitude molecular motions has a strong effect on NMR spectra. Motional rates much higher than that of the rigid-limit nuclear spin interaction of interest scale the interaction and cause spectral narrowing, while rates similar to the NMR interaction strengths cause severe line broadening and intensity loss (10). Saffman and Delbruck considered Brownian motions of proteins in lipid bilayers (11) and concluded that the rotational diffusion rates,  $D_R$ , of membrane proteins around the bilayer normal depend on the viscosity of the bilayer and the

volume of the membrane protein. For a cylindrical protein traversing the bilayer, the rotational diffusion rate is directly proportional to temperature ( $T$ ) and inversely proportional to the membrane viscosity ( $\eta$ ), thickness ( $h$ ), and the square of the radius ( $r$ ) of the cylinder ( $D_R = KT/4\pi\eta r^2 h$ ) (11). The equation predicts that in DLPC<sup>1</sup> bilayers with  $\eta = 5 \text{ P}$  at 298 K, a transmembrane (TM) helical bundle with a radius of 12.5 Å has a rotational diffusion rate of  $\sim 1 \times 10^5 \text{ s}^{-1}$ , which is larger than those of most NMR interactions. Indeed, motionally averaged  $^2\text{H}$  quadrupolar couplings,  $^{13}\text{C}-^1\text{H}$  and  $^{15}\text{N}-^1\text{H}$  dipolar couplings, and  $^{13}\text{C}$  chemical shift anisotropies were observed for a TM helical bundle (12).

While this uniaxial diffusion stems from general physical principles and has practical benefits such as enabling orientation determination (12), it can also complicate solid-state NMR structure determination of membrane proteins due to intermediate time scale line broadening at ambient temperature. While one can overcome this line broadening by freezing the membrane samples, low-temperature NMR often yields lower-resolution

<sup>†</sup>This work is supported by National Science Foundation Grant MCB-0543473.

\*To whom correspondence should be addressed. E-mail: mhong@iastate.edu. Telephone: (515) 294-3521. Fax: (515) 294-0105.

<sup>1</sup>Abbreviations: DPPC, 1,2-dipalmitoyl-*sn*-glycerol-3-phosphocholine; DPPE, 1,2-dipalmitoyl-*sn*-glycerol-3-phosphoethanolamine; DLPC, 1,2-dilauroyl-*sn*-glycerol-3-phosphocholine; DMPC, 1,2-dimyristoyl-*sn*-glycerol-3-phosphocholine; POPC, 1-palmitoyl-2-oleoyl-*sn*-glycerol-3-phosphocholine; PC, phosphocholine; PE, phosphoethanolamine.

spectra compared to the spectra of rigid solids at ambient temperature. Moreover, the low-temperature protein structure may differ from its structure at physiological temperature. Thus, there is a strong incentive to develop alternative methods for creating well-ordered and immobilized membrane proteins at physiological temperature.

The M2 proteins of influenza A and B viruses (AM2 and BM2) are integral membrane proteins that form pH-activated proton channels essential for virus replication (13, 14). As the smallest ion channel proteins that have complete ion selectivity and activation properties, the M2 proteins are excellent model systems for understanding the effects of lipid membranes on protein structure and dynamics. AM2 is the target of the antiviral drug amantadine (15, 16). Thus, elucidating the influence of the lipid membrane on M2 structure and dynamics also has public health importance. The AM2 transmembrane (TM) domain structure has been extensively studied in simple PC bilayers using solid-state NMR (SSNMR). These spectra, measured both under static aligned conditions and under magic-angle spinning (MAS), clearly show that AM2-TM undergoes extensive conformational motion in the liquid-crystalline phase of DLPC, DMPC, and POPC bilayers (12, 17). The main motion is uniaxial rotational diffusion of the helical bundle relative to the bilayer normal, as evidenced by  $^{15}\text{N}$  NMR spectra (12, 18). As the temperature decreases, the motion slows, giving rise to exchange-broadened spectra at intermediate temperatures ( $\sim 293$  K) (17) and slow-limit high-intensity spectra at low temperatures ( $\sim 243$  K). More recently, the structure of TM-containing domains of AM2 was determined by X-ray crystallography in the detergent octyl  $\beta$ -D-glucopyranoside (19) and by solution NMR in DHPC micelles (20). The detergent environment created dynamic difficulties for solution NMR experiments, as manifested by broad lines under certain conditions. Most importantly, the two structures differ dramatically in the drug-binding site and also noticeably in the helix orientation, thus underscoring the importance of further investigating the M2 transmembrane structure in native-like lipid bilayers (21).

While detergents are known to be limited mimetics of lipid bilayers, even the lipid bilayers used so far in SSNMR experiments to characterize the AM2-TM structure do not resemble the native virus envelope. The influenza virus envelope membrane contains significant amounts of cholesterol (Chol), saturated-chain PC and PE lipids, and sphingomyelin (SM) (22). This composition is characteristic of eukaryotic cell membranes, because the virus takes the lipids from its host cells. In this work, we show that the AM2-TM rotational diffusion is slowed by 2 orders of magnitude in a sphingomyelin- and cholesterol-rich synthetic membrane that mimics the virus and eukaryote lipid membranes (termed "viral membrane" below). This immobilization yields high-resolution solid-state NMR spectra at ambient temperature and allows interatomic distances to be measured without freezing the sample. We can largely account for the immobilization by the significantly increased viscosity of the virus-mimetic membrane. Second, we examined the conformation of various residues of AM2-TM in this viral membrane using two-dimensional (2D)  $^{13}\text{C}$  and  $^{15}\text{N}$  NMR. We find that except for lipid-facing side chains and known hot spots of conformational change in the protein, the average conformation of most residues is not changed from that in model membranes. Thus, this eukaryote-mimetic lipid membrane offers significant biological and NMR spectroscopic advantages for structure determination.

## MATERIALS AND METHODS

**Membrane Sample Preparation.** The TM domain of the M2 protein of the Udorn strain (residues 22–46, SSDPLVVAA-SIIGILHLILWILDRL) was synthesized by Fmoc chemistry and purified to  $>95\%$  purity. Two peptide samples containing eight uniformly  $^{13}\text{C}$ - and  $^{15}\text{N}$ -labeled residues were used. The labeled sites are L26, A29, G34, and I35 in one sample (LAGI) and V27, A30, I33, and L38 in the other (VAIL).

Egg sphingomyelin (SM) was dissolved in a chloroform/methanol (10:2) solution and mixed with DPPC, DPPE, and cholesterol (Chol) at an SM:DPPC:DPPE:Chol molar ratio of 28:21:21:30. The membrane mixture was lyophilized, dissolved in pH 7.5 phosphate buffer, vortexed, and frozen and thawed several times to form large unilamellar vesicles. The membrane has a broad phase transition around 243 K based on static  $^{31}\text{P}$  spectra (Figure S1 of the Supporting Information).

AM2-TM was reconstituted into the viral membrane mixture by detergent dialysis as described previously (23). The peptide:lipid molar ratios were from 1:15 to 1:12. The proteoliposomes were centrifuged at 150000g to yield the membrane pellet. The photometric assay showed  $>95\%$  binding of the peptide. The pellet was packed into 4 mm MAS rotors for NMR experiments. For the amantadine-bound sample, amantadine hydrochloride in the pH 7.5 buffer was directly titrated to the pellet at a peptide:amantadine molar ratio of 1:2.

**Solid-State NMR.** SSNMR experiments were conducted on 400 MHz (9.4 T) and 600 MHz (14.1 T) spectrometers using 4 mm MAS probes. Experiments on viral membrane samples were conducted near 303 K, well above the phase transition temperature.  $^{15}\text{N}$ - $^1\text{H}$  and  $^{13}\text{C}$ - $^1\text{H}$  dipolar couplings were measured using either the dipolar-doubled DIPSHIFT experiments under 7 kHz MAS (24) or the 2D LG-CP experiment under 10 kHz MAS. For the DIPSHIFT experiment, an FSLG sequence was used for  $^1\text{H}$  homonuclear decoupling. The time domain data were fit to give the apparent coupling strengths, which were then divided by  $2 \times 0.577$  to take into account the dipolar doubling and the scaling factor of FSLG. The true couplings were divided by the rigid-limit couplings to obtain the order parameters,  $S_{\text{CH}}$  and  $S_{\text{NH}}$ . Thus, the order parameter depends on the product of the scaling factor and the rigid-limit dipolar coupling, both of which contain uncertainties due to experimental imperfections and vibrational averaging, respectively. We used the model peptide  $^{13}\text{C}$ - and  $^{15}\text{N}$ -labeled formyl-MLF to calibrate the DIPSHIFT experiments and found that with a rigid-limit coupling of 10.5 kHz for N-H coupling, 22.7 kHz for C-H coupling, and the theoretical scaling factor of 0.577 (25), reasonable order parameters are found for formyl-MLF (0.95–1.0). Thus, these rigid-limit coupling values and the scaling factor were used for extracting the order parameters of AM2-TM.

2D  $^{15}\text{N}$ - $^{13}\text{C}$  correlation spectra (26) were recorded under 7 kHz MAS using a REDOR pulse train (27) of 0.7 ms for  $^{13}\text{C}$ - $^{15}\text{N}$  coherence transfer. Typical radiofrequency fields were 50 kHz for  $^{13}\text{C}$  and  $^{15}\text{N}$  and 60–70 kHz for  $^1\text{H}$ .  $^{13}\text{C}$  and  $^{15}\text{N}$  chemical shifts were referenced to the  $\alpha$ -Gly CO signal at 176.49 ppm on the TMS scale and the  $^{15}\text{N}$  signal of *N*-acetylvaline at 122 ppm on the liquid ammonia scale, respectively.

## RESULTS

**Calculated Rotational Diffusion Rates of Membrane Proteins in Viral Membranes.** The lipid composition of the influenza virus envelope resembles the host cell membrane from

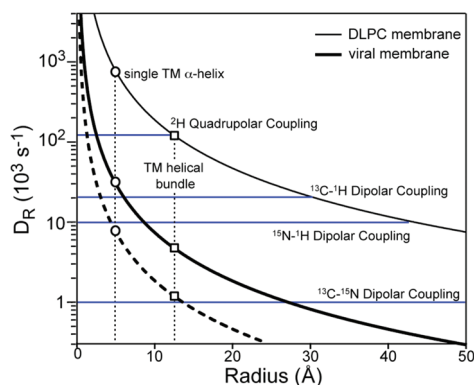


FIGURE 1: Calculated rotational diffusion rates ( $D_R$ ) of membrane proteins in viral membranes (thick line) and DLPC bilayers (thin line) at 298 K. The DLPC curve was calculated with an  $\eta$  of 5 P and an  $h$  of 35 Å. The viral membrane curve was calculated with an  $\eta$  of 100 P and an  $h$  of 45 Å. The dashed line was calculated with an  $\eta$  of 400 P and an  $h$  of 45 Å. The radii of a single TM helix and a TM helical bundle are 5 and 12.5 Å, respectively. The sizes of several NMR spin interactions are shown as blue horizontal lines.

which it buds and contains SM, PC, and PE lipids (22). Together, they account for 70–80% of the total lipid mass (28). The lipid chains are largely saturated with 16 or 18 carbons (29). Cholesterol is abundant in the virus envelope. The lipid:Chol mass ratio is 2–3, depending on the host cell, the nature of the virus, and the presence of small molecules such as vitamin A (29). SM and Chol-rich lipid membranes have been extensively studied for their role in raft formation (30), and diffusion coefficients, membrane thickness, and headgroup area per lipid have been estimated (31). The virus–mimetic membrane is generally more viscous, thicker, and denser than one-component low-melting PC bilayers.

Figure 1 plots the calculated protein rotational diffusion rates ( $D_R$ ) at 298 K in DLPC bilayers and viral membranes as a function of the protein radius. The main parameter affecting the rotational diffusion rate is the viscosity,  $\eta$ . Low-melting PC bilayers have an  $\eta$  of 1–10 P (11, 32). We used an  $\eta$  of 5 P to calculate the  $D_R$  in DLPC bilayers. For SM and Chol-rich viral membranes, the viscosities were estimated to be at least 20-fold higher than those of simple PC membranes based on pulse field gradient NMR (33) and molecular dynamics simulations (31). Thus, we used an  $\eta$  of 100 P to calculate  $D_R$  in the viral membrane. The bilayer thickness,  $d_{pp}$ , is  $\sim 35$  Å for DLPC and  $\sim 45$  Å for the viral membrane. The resulting  $D_R$  curves show the expected difference between the two membranes. A single TM helix (radius = 5 Å) has a  $D_R$  of  $\approx 7 \times 10^5$  s $^{-1}$  in DLPC bilayers but only  $3 \times 10^4$  s $^{-1}$  in the viral membrane. Thus, a TM helix should have rigid-limit  $^2\text{H}$  couplings in the viral membrane but motionally averaged  $^{13}\text{C}$  and  $^{15}\text{N}$  dipolar and chemical shift spectra. For a TM helical bundle (radius = 12.5 Å),  $D_R$  is  $\sim 1 \times 10^5$  s $^{-1}$  in DLPC bilayers but only  $5 \times 10^3$  s $^{-1}$  in the viral membrane. Thus, the helical bundle should exhibit rigid-limit spectra for not only  $^2\text{H}$  quadrupolar interactions but also  $^{13}\text{C}$ – $^1\text{H}$  and  $^{15}\text{N}$ – $^1\text{H}$  dipolar interactions. Whether the one-bond  $^{13}\text{C}$ – $^{15}\text{N}$  dipolar coupling, which is only  $\sim 1$  kHz in the rigid limit, will be motionally averaged depends on the accuracy of the viscosity estimate. We will directly test these predictions by experiments below.

**Observed AM2-TM Immobilization in Viral Membranes.** Figure 2 shows the  $^2\text{H}$  spectra of two Ala CD $_3$  sites in AM2-TM reconstituted into viral and DLPC membranes. Ala CD $_3$  quadrupolar couplings reflect the dynamics of the C $\alpha$ –C $\beta$  bond (34). Fast motions additional to methyl three-site jumps are

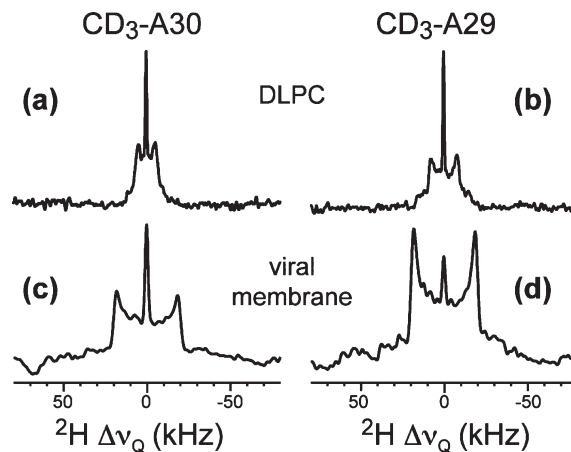


FIGURE 2:  $^2\text{H}$  spectra of Ala CD $_3$ -labeled AM2-TM in different lipid membranes at pH 7.5 and 313 K: (a) DLPC bilayers, A30 CD $_3$ ; (b) DLPC bilayers, A29 CD $_3$ ; (c) viral membrane, A30 CD $_3$ ; and (d) viral membrane, A29 CD $_3$ .

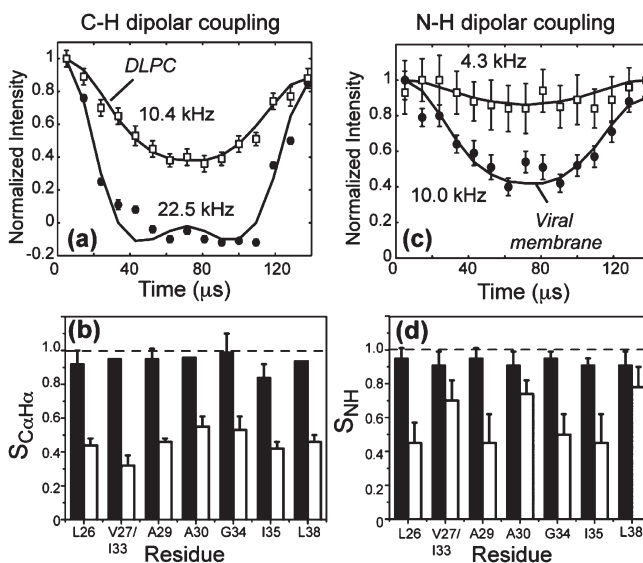


FIGURE 3: C–H and N–H dipolar couplings of AM2-TM in different membranes at 313 K: (●) viral membrane data and (□) DLPC data. (a) A29 C $\alpha$ –H $\alpha$  dipolar coupling. (b) C $\alpha$ –H $\alpha$  order parameters of AM2-TM in viral membranes (black bars) and DLPC bilayers (white bars). (c) L26 N–H dipolar coupling. (d) N–H order parameters in viral membranes (black bars) and DLPC bilayers (white bars). The couplings indicated in panels a and c are true couplings after the scaling factors have been taken into account.

manifested as couplings of  $< 40$  kHz. For DLPC-bound samples, the  $^2\text{H}$  splittings are 10.0 kHz for A30 and 15.7 kHz for A29 at 313 K (12), indicating that the helix backbone undergoes rotational diffusion at rates much faster than  $4 \times 10^4$  s $^{-1}$ . In contrast, in the viral membrane, both methyl groups show  $^2\text{H}$  splittings of 37.6 kHz at 313 K. Thus, the M2 backbone is immobilized in the viral membrane to  $< 4 \times 10^4$  s $^{-1}$ . The remaining scaling factor of 0.94 reflects small-amplitude local motions.

To determine if AM2-TM diffuses at rates slower than  $4 \times 10^4$  s $^{-1}$ , we measured the C–H and N–H dipolar couplings and compared them with the rigid-limit couplings obtained from model compounds. Figure 3 shows selected C $\alpha$ –H $\alpha$  and N–H dipolar DIPSHIFT curves at 313 K for DLPC- and viral membrane-bound AM2-TM. For all residues, the viral membrane samples exhibit nearly rigid-limit couplings whereas the DLPC samples

Table 1: C–H and N–H Order Parameters of Labeled Residues in AM2-TM Bound to Virus Envelope Mimetic Membrane versus DLPC Bilayers at 313 K

residue	$S_{CH}$		$S_{NH}$	
	viral	DLPC	viral	DLPC
L26	0.92	0.44	0.95	0.45
V27/I33	0.95	0.32	0.91	0.70
A29	0.95	0.46	0.95	0.45
A30	0.96	0.55	0.91	0.74
G34	0.99	0.53	0.95	0.50
I35	0.84	0.42	0.91	0.45
L38	0.94	0.46	0.91	0.78

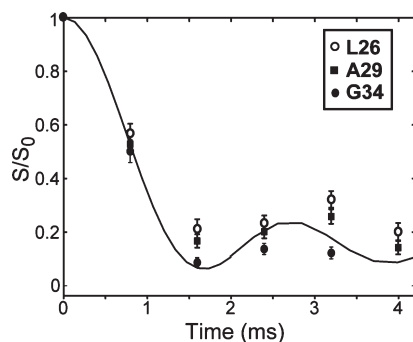


FIGURE 4:  $^{13}\text{C}$ – $^{15}\text{N}$  dipolar couplings of LAGI-M2 in viral membranes at 303 K. The calculated REDOR curve is for a 1.0 kHz dipolar coupling.

show much smaller couplings that are indicative of large-amplitude motions. The C–H order parameters range from 0.84 to 0.99 for the viral membrane-bound peptide but only from 0.32 to 0.55 for the DLPC-bound M2, while the N–H order parameters range from 0.91 to 0.95 for the viral membrane sample and only from 0.45 to 0.78 for the DLPC-bound peptide (Table 1). The high order parameters of the viral membrane samples are consistent with the suppression of the whole-body motion and the presence of only small segmental motion, with I35 showing particular local flexibility. Thus, AM2-TM is immobilized to  $< 1 \times 10^4 \text{ s}^{-1}$  in the viral membrane.

To place a tighter upper limit to the motional rates of AM2-TM in the viral membrane, we measured an even smaller spin interaction, the one-bond  $^{15}\text{N}$ – $^{13}\text{C}\alpha$  dipolar coupling, which has a rigid limit of  $\sim 1.0 \text{ kHz}$ . Using a  $^{13}\text{C}$  homonuclear decoupled  $^{13}\text{C}$ – $^{15}\text{N}$  REDOR experiment (35), we obtained REDOR dephasing curves of several C $\alpha$  sites, as shown in Figure 4. The first intensity minimum appears at 1.6 ms, which is approximately the time expected for the rigid-limit  $^{15}\text{N}$ – $^{13}\text{C}\alpha$  coupling. Thus, AM2-TM is immobilized to  $< 10^3 \text{ s}^{-1}$ .

**Effect of M2 Immobilization on  $^{13}\text{C}$  and  $^{15}\text{N}$  NMR Spectra.** The two orders of magnitude decrease in motional rates by the viral membrane gives rise to slow-limit  $^{13}\text{C}$  and  $^{15}\text{N}$  NMR spectra of AM2-TM with high intensities and narrow lines at ambient temperature. Figure 5 compares the AM2-TM  $^{13}\text{C}$  cross-polarization (CP) spectra in the viral membrane and in the DLPC bilayer. The viral membrane samples give strong and narrow backbone C $\alpha$  signals from 303 to 243 K, and the intensities increase monotonically with a decrease in temperature, consistent with the Boltzmann law. The same trend is observed in the  $^{15}\text{N}$  spectra (Figure S2 of the Supporting Information). In contrast, the DLPC samples have minimum backbone intensities

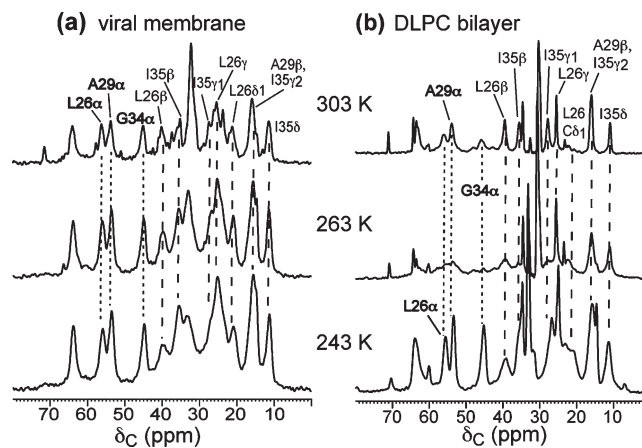


FIGURE 5:  $^{13}\text{C}$  CP-MAS spectra of amantadine-bound LAGI AM2-TM in two different membranes at 303, 263, and 243 K: (a) viral membrane and (b) DLPC bilayers. The peptide shows stronger and narrower lines in the viral membrane than in DLPC bilayers at physiological temperature.

at intermediate temperatures of  $\sim 263 \text{ K}$  and higher intensities at 243 and 303 K, indicating intermediate time scale motional broadening at 263 K.

The side-chain  $^{13}\text{C}$  signals in Figure 5 have high intensities in both bilayers, but the line widths are slightly larger in the viral membrane. This is due to fast torsional motions of the side chains in addition to the backbone motion. When the helical backbone diffuses on the intermediate time scale in DLPC bilayers, the combined motion of the side chains is fast, giving rise to narrow lines. When the backbone is immobilized in the viral membrane, the side chains have slightly slower motions, thus giving slightly broader lines, but in neither bilayer do the side-chain motions fall outside the fast limit; thus, high sensitivity is observed in both membranes. Since the side-chain NMR signals usually do not suffer from line broadening due to the fast segmental motions, we do not concern ourselves with these signals further.

To examine whether the change in membrane composition affects the peptide conformation, we compared 2D  $^{13}\text{C}$ – $^{13}\text{C}$  and  $^{13}\text{C}$ – $^{15}\text{N}$  correlation spectra of AM2-TM in the viral and DLPC membranes. Figure S3 of the Supporting Information shows regions of the 2D  $^{13}\text{C}$ – $^{13}\text{C}$  spectra where most sites exhibit small chemical shift changes ( $< 0.5 \text{ ppm}$ ). The main exception is I33, whose side-chain carbons have chemical shift changes of 0.4–1.9 ppm. This is consistent with the lipid-facing location of I33 (36), which makes this site sensitive to the membrane composition change. In comparison, channel-facing residues such as A30 and G34 have minimal  $^{13}\text{C}$  chemical shift changes between the two membranes.

For the pore-facing V27, the C $\alpha$  chemical shift decreased by 1.5 ppm while the C' chemical shift increased by 1.0 ppm compared to the DLPC values. The V27 conformation and dynamics are known to be sensitive to drug binding (37) and pH (38). MD simulations suggest that at low external pH the V27 region adopts a closed conformation whereas at high pH the V27 region opens. This pH-dependent V27 gate, together with the NMR-detected drug binding sensitivity and membrane sensitivity, indicates that V27 is a hot spot of conformational change in response to the environment.

$^{15}\text{N}$  chemical shifts are generally more sensitive to the conformation and the electrostatic environment of protein residues. Indeed, the 2D  $^{15}\text{N}$ – $^{13}\text{C}$  correlation spectra of AM2-TM under different conditions show significant  $^{15}\text{N}$  line width differences.

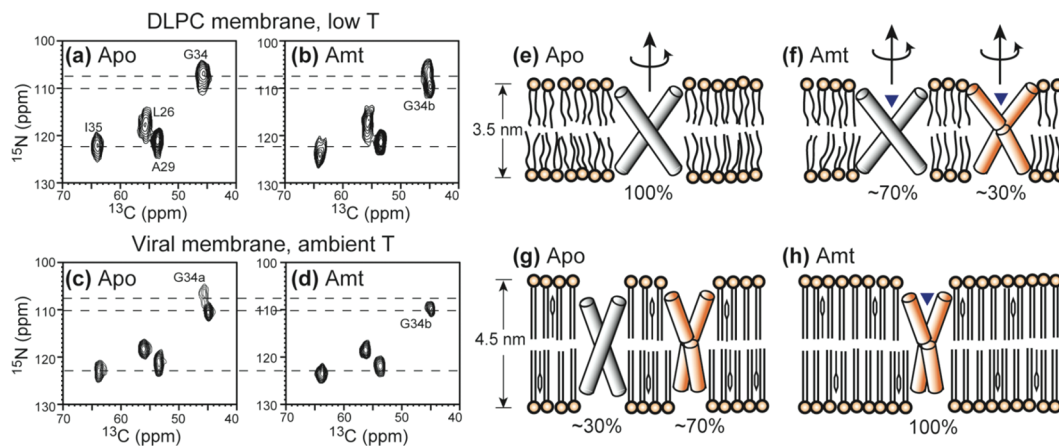


FIGURE 6: 2D  $^{15}\text{N}$ – $^{13}\text{C}$  HETCOR spectra of LAGI AM2-TM in different membranes and drug binding states. (a) Apo AM2-TM in DLPC bilayers at 243 K. (b) Amantadine-bound AM2-TM in DLPC bilayers at 243 K. (c) Apo AM2-TM in viral membranes at 294 K. (d) Amantadine-bound AM2-TM in viral membranes at 303 K. The corresponding helix orientations are shown at the right. (e) Apo peptide in DLPC bilayers. The helices are straight and tilted by  $35^\circ$  from the bilayer normal (37). (f) Amantadine-bound peptide in DLPC bilayers. Approximately thirty percent of the helices exhibit a kink of  $10^\circ$  at G34. (g) Apo peptide in the viral membrane. Approximately seventy percent of the helices have the kinked conformation. (h) Amantadine-bound peptide in the viral membrane. All helices have the kinked conformation.

Figure 6 compares the 2D  $^{15}\text{N}$ – $^{13}\text{C}$  spectra for the peptide in DLPC bilayers and in viral membranes, both without amantadine and with amantadine. All spectra were measured on immobilized protein, which is achieved by cooling to 243 K for the DLPC samples, but at  $\sim 303$  K for the viral membrane samples. It can be seen that the ambient-temperature viral membrane samples give much narrower  $^{15}\text{N}$  lines than the frozen DLPC samples, indicating high conformational homogeneity of the protein in the viral membrane. In addition, the G34  $^{15}\text{N}$  peak shows interesting dependences on the membrane composition and drug binding state. In DLPC bilayers, the peak is broad (107.0 ppm) without the drug, split into two peaks, G34a (106.3 ppm) and G34b (109.7 ppm), after amantadine binding. In the viral membrane, the G34  $^{15}\text{N}$  signal has the same two-peak pattern in the absence of drug but changes to a single peak at the downfield position (G34b) in the presence of amantadine. Thus, the viral membrane and amantadine both induce the downfield  $^{15}\text{N}$  chemical shift, so that under the combined effects of the two, the G34b conformer dominates. Moreover, the fact that amantadine changes the G34  $^{15}\text{N}$  chemical shift in the same direction (downfield by  $\sim 2.7$  ppm) in the viral membrane and in the DLPC bilayer indicates that the peptide is similarly sensitive to amantadine in both membranes. This is consistent with analytical ultracentrifugation data showing amantadine binding of AM2-TM in cholesterol-containing membranes.

## DISCUSSION

The main observation from the data given above is that the AM2-TM peptide is nearly fully immobilized in the virus envelope–mimetic lipid membrane at physiological temperature, in dramatic contrast to high peptide dynamics in DLPC, DMPC, and POPC membranes. The  $^2\text{H}$  quadrupolar spectra and  $^{13}\text{C}$ – $^1\text{H}$ ,  $^{15}\text{N}$ – $^1\text{H}$ , and  $^{13}\text{C}$ – $^{15}\text{N}$  dipolar couplings indicate unequivocally that the  $\gg 4 \times 10^4 \text{ s}^{-1}$  rotational diffusion of AM2-TM in DLPC bilayers is slowed to  $< 1$  kHz in the eukaryote– and virus–mimetic membrane at physiological temperature. This immobilization narrowed and increased the backbone  $^{13}\text{C}$  and  $^{15}\text{N}$  signals where previously no signals could be observed due to intermediate time scale motion (12). The dramatic immobilization of the AM2-TM helical bundle by 2 orders of magnitude is largely ascribed to the increased viscosity

and thickness of the viral membrane over model PC membranes (Figure 1). The calculated diffusion rate based on the simple hydrodynamic model for two-dimensional fluids agrees remarkably well with the experimental results. The fact that the M2 helical bundles are measured to be immobilized down to  $\sim 1$  kHz while the Saffman–Delbruck equation predicted immobilization to  $\sim 5$  kHz most likely reflects uncertainties in the membrane viscosity and in the estimated helical bundle radius. It is unlikely for specific cholesterol binding to be the cause of this immobilization, since the number of cholesterol molecules bound per M2 tetramer has been estimated to be only 0.5–0.9 (39, 40). Moreover, the immobilization is observed for all labeled residues in the protein and thus reflects the property of the whole peptide, rather than a local effect as would be expected for specific cholesterol binding.

It is important to use the TM peptide as a template for investigating the effects of the viral membrane on the M2 physical property, since abundant NMR data are available on this TM peptide bound to simple model membranes. Moreover, recent electrophysiological data in oocytes have shown that the TM domain is the functional core of M2, containing all the hallmarks of M2 functions: tetramer assembly, proton transport, pH gating, ion selectivity, and drug binding (41). Whether similar immobilization will occur for full-length M2 will require future studies, since few NMR data on the intact protein in solution or in the solid state are available. It is possible that the intact protein may already be largely immobilized in model membranes because of its higher molecular weight. However, the structural ordering effect of the cholesterol-rich viral membrane should persist and thus should still create a more homogeneous conformation for the full-length protein.

The substantial change in the AM2-TM helical bundle dynamics is consistent with the structural plasticity of AM2-TM, which has been well documented by the sensitivity of helix orientation (12, 42–44) and conformation (37, 45) to membrane thickness, drug binding, and pH.

The extent of AM2-TM tetramerization is also environment-dependent: lipid bilayers create much more stable tetramers than detergents, and thicker bilayers and cholesterol-containing bilayers stabilize tetramers more than thin bilayers without cholesterol (39). Tetramer formation also depends on the peptide

concentration (46, 47): at the high peptide:lipid molar ratios (~1:15) used in most solid-state NMR experiments AM2-TM exists almost exclusively in the tetramer state in the tetramer–monomer equilibrium, as shown by  $^{19}\text{F}$  spin diffusion NMR data (48, 49) and analytical ultracentrifugation data (46). Taken together, these data indicate that both in simple PC membranes and in the complex viral membranes, the oligomeric state of AM2-TM is tetrameric and is not the cause of the dynamics change.

The ability of the eukaryote–mimetic viral membrane to immobilize a classical TM helical bundle (50) at physiological temperature offers significant opportunities for structure determination of membrane proteins by solid-state NMR. So far with few exceptions (51), membrane protein SSNMR studies that involve synthetic lipids use one- or two-component lipid bilayers without cholesterol, which create unfavorable dynamic properties of proteins that need to be remedied by low-temperature experiments. In cases where more native membrane extracts were used, the most common choices are *Escherichia coli* lipids (52), asolectin (53), and purple membrane lipids (54, 55), none of which have the immobilizing properties of the viral membrane. The purple membrane is noteworthy, as it is the matrix in which bacteriorhodopsin (bR) forms immobile trimeric crystalline arrays. However, the purple membrane consists of ether-linked diphytanoyl lipids that do not have a phase transition between  $-120$  and  $80$  °C (56). bR immobilization is thus due to its dense packing, despite the fluidity of the purple membrane. The virus envelope–mimetic membrane is the only membrane composition identified so far to directly immobilize proteins. This membrane mixture contains a high percentage of cholesterol (30 mol %) and does not have unsaturated lipids. Both factors suppress domain formation (57), so that the membrane is most likely in a single liquid-ordered phase. This is supported by the  $^{31}\text{P}$  static spectra, which show a single chemical shift anisotropy pattern at each temperature (Figure S1 of the Supporting Information). Irrespective of the detailed physical properties of this membrane, the fact that it suppresses whole-body motion and consequently enhances NMR spectral resolution and sensitivity is unambiguous. Structure determination of eukaryotic membrane proteins is thus both more biological and more favorable for solid-state NMR in this membrane mixture.

The effects of the viral membrane on the AM2-TM conformation are interesting.  $^{13}\text{C}$  and  $^{15}\text{N}$  chemical shifts indicate that the viral membrane does not affect the average conformation (peak position) of most sites except for lipid-exposed side chains but reduces the conformational heterogeneity of the protein. The latter is manifested by the narrow line widths of the room-temperature spectra of the protein in the viral membrane compared to those observed in frozen PC membranes (Figure 6). The viral membrane may reduce the protein conformational distribution by virtue of its larger viscosity, which creates a higher energy barrier for conformational excursion of the protein. The line narrowing may also partly result from small-amplitude local motion of the protein, as manifested by the 5–10% lower order parameters from the rigid-limit value of 1.0 (Figure 3).

At 243 K, in the gel phase of the viral lipid membrane, the protein shows  $^{15}\text{N}$  spectra similarly broadened compared to those of the frozen DLPC-bound M2 samples (Figure S2 of the Supporting Information). We hypothesize that the significantly altered lipid environment below the phase transition causes heterogeneity in the protein, whether it is in the viral membranes or in the one-component PC membranes. It should be mentioned that such low-temperature line broadening, which

has been widely observed in SSNMR spectra, is still poorly understood, and further studies are necessary to elucidate the contributions to low-temperature line widths.

The observed chemical shift perturbation of G34 and V27 by the membrane composition change is unlikely to be due to specific cholesterol binding, again because of the very small number of cholesterol molecules bound per tetramer (39, 40). Instead, it most likely reflects the intrinsic conformational flexibility of G34 and V27 in response to the environment. G34 is the site at which a helix kink of  $\sim 15^\circ$  was observed as a result of amantadine binding (43), where the C-terminal segment became less tilted than the N-terminal segment. By inference, the downfield  $^{15}\text{N}$  isotropic peak upon amantadine binding (Figure 6) is also due to the kinked helices. This means that the two G34  $^{15}\text{N}$  peaks in the apo viral membrane result from the coexistence of straight and kinked helices, which is also suggested by static  $^{15}\text{N}$  spectra of apo M2 in oriented DMPC membranes (17). The growth of kinked and less tilted helices is consistent with the larger thickness of the viral membrane, by reducing the hydrophobic mismatch between the protein and the membrane. Since amantadine and the viral membrane affect the helix orientation in the same direction, the drug-complexed peptide in the viral membrane shows only the kinked conformation. Figure 6e–h depicts the proposed AM2-TM orientations under the four membrane–drug conditions, where the populations of the straight and kinked helices are estimated from the relative intensities of the two G34 peaks in the 2D spectra. The fact that the G34  $^{15}\text{N}$  chemical shift in the viral membrane is perturbed by amantadine in the same direction as the peptide in the DLPC bilayer also indicates that the peptide retains the similar amantadine sensitivity as in model membranes.

In influenza-infected host cells, the M2 protein does not concentrate in raft-like microdomains but is thought to prefer the raft–nonraft interface, in contrast to hemagglutinin and neuraminidase, which localize in detergent-resistant membranes (40, 58). However, in the virus envelope, the level of M2 protein is known to be low, indicating that the virus envelope presents little disordered phase into which M2 can partition and that most M2 proteins reside in a liquid-ordered phase similar to that used here. Therefore, studies of M2 proteins in cholesterol-rich membranes are biologically relevant, in addition to being spectroscopically favorable.

In conclusion, a membrane mixture mimicking the eukaryotic cell membrane in general and the influenza virus envelope composition in particular is found to immobilize the whole-body uniaxial rotation of the M2 transmembrane helical bundle. The use of this cholesterol-rich eukaryotic membrane mixture should greatly facilitate solid-state NMR structure determination of membrane proteins in lipid bilayers, by allowing experiments to be conducted near physiological temperature without dynamic broadening, giving significantly enhanced spectral resolution and sensitivity. The reduction of dynamic disorder by the addition of cholesterol may also be relevant for X-ray crystallography of membrane proteins. This study underscores the importance of studying membrane proteins in the most native lipid membrane.

#### SUPPORTING INFORMATION AVAILABLE

$^{31}\text{P}$  spectra of the viral membrane,  $^{15}\text{N}$  one-dimensional variable-temperature spectra, and 2D  $^{13}\text{C}$ – $^{13}\text{C}$  correlation spectra of AM2-TM. This material is available free of charge via the Internet at <http://pubs.acs.org>.

## REFERENCES

- (1) Hong, M. (2006) Oligomeric structure, dynamics, and orientation of membrane proteins from solid-state NMR. *Structure* 14, 1731–1740.
- (2) Hong, M. (2007) Structure, topology, and dynamics of membrane peptides and proteins from solid-state NMR spectroscopy. *J. Phys. Chem. B* 111, 10340–10351.
- (3) Reuther, G., Tan, K. T., Vogel, A., Nowak, C., and Arnold, K.; et al. (2006) The lipidated membrane anchor of full length N-Ras protein shows an extensive dynamics as revealed by solid-state NMR spectroscopy. *J. Am. Chem. Soc.* 128, 13840–13846.
- (4) Park, S. H., Mrse, A. A., Nevzorov, A. A., De Angelis, A. A., and Opella, S. J. (2006) Rotational diffusion of membrane proteins in aligned phospholipid bilayers by solid-state NMR spectroscopy. *J. Magn. Reson.* 178, 162–165.
- (5) Hong, M. (2006) Solid-state NMR studies of the structure, dynamics, and assembly of  $\beta$ -sheet membrane peptides and  $\alpha$ -helical membrane proteins with antibiotic activities. *Acc. Chem. Res.* 39, 176–183.
- (6) Luo, W., Yao, X. L., and Hong, M. (2005) Large Structure Rearrangement of Colicin Ia Channel Domain After Membrane Binding from 2D  $^{13}\text{C}$  Spin Diffusion NMR. *J. Am. Chem. Soc.* 127, 6402–6408.
- (7) Huster, D., Xiao, L. S., and Hong, M. (2001) Solid-State NMR Investigation of the dynamics of colicin Ia channel-forming domain. *Biochemistry* 40, 7662–7674.
- (8) Tang, M., Waring, A. J., Lehrer, R. I., and Hong, M. (2008) Effects of Guanidinium-Phosphate Hydrogen Bonding on the Membrane-Bound Structure and Activity of an Arginine-Rich Membrane Peptide from Solid-State NMR. *Angew. Chem., Int. Ed.* 47, 3202–3205.
- (9) Doherty, T., Waring, A. J., and Hong, M. (2008) Dynamic structure of disulfide-removed linear analogs of tachyplesin-I in the lipid bilayer from solid-state NMR. *Biochemistry* 47, 1105–1116.
- (10) Bain, A. D. (2003) Chemical exchange in NMR. *Prog. Nucl. Magn. Reson. Spectrosc.* 43, 63–103.
- (11) Saffman, P. G., and Delbruck, M. (1975) Brownian motion in biological membranes. *Proc. Natl. Acad. Sci. U.S.A.* 72, 3111–3113.
- (12) Cady, S. D., Goodman, C., Tatko, C., DeGrado, W. F., and Hong, M. (2007) Determining the orientation of uniaxially rotating membrane proteins using unoriented samples: A  $^2\text{H}$ ,  $^{13}\text{C}$ , and  $^{15}\text{N}$  solid-state NMR investigation of the dynamics and orientation of a transmembrane helical bundle. *J. Am. Chem. Soc.* 129, 5719–5729.
- (13) Pinto, L. H., Holsinger, L. J., and Lamb, R. A. (1992) Influenza virus M2 protein has ion channel activity. *Cell* 69, 517–528.
- (14) Pinto, L. H., and Lamb, R. A. (2007) Controlling influenza virus replication by inhibiting its proton flow. *Mol. BioSyst.* 3, 18–23.
- (15) Hay, A. J., Wolstenholme, A. J., Skehel, J. J., and Smith, M. H. (1985) The molecular basis of the specific anti-influenza action of amantadine. *EMBO J.* 4, 3021–3024.
- (16) Wang, C., Takeuchi, K., Pinto, L. H., and Lamb, R. A. (1993) Ion Channel Activity of Influenza A Virus M2 Protein: Characterization of the Amantadine Block. *J. Virol.* 67, 5585–5594.
- (17) Li, C., Qin, H., Gao, F. P., and Cross, T. A. (2007) Solid-state NMR characterization of conformational plasticity within the transmembrane domain of the influenza A M2 proton channel. *Biochim. Biophys. Acta* 1768, 3162–3170.
- (18) Kovacs, F. A., and Cross, T. A. (1997) Transmembrane four-helix bundle of influenza A M2 protein channel: Structural implications from helix tilt and orientation. *Biophys. J.* 73, 2511–2517.
- (19) Stouffer, A. L., Acharya, R., Salom, D., Levine, A. S., and Di Costanzo, L.; et al. (2008) Structural basis for the function and inhibition of an influenza virus proton channel. *Nature* 451, 596–599.
- (20) Schnell, J. R., and Chou, J. J. (2008) Structure and mechanism of the M2 proton channel of influenza A virus. *Nature* 451, 591–595.
- (21) Miller, C. (2008) Ion channels: Coughing up flu's proton channels. *Nature* 451, 532–533.
- (22) Klenk, H. D., Becht, H., and Rott, R. (1972) Structure of Influenza-Virus Envelope. *Virology* 47, 579–591.
- (23) Cady, S. D., Mishanina, T. V., and Hong, M. (2009) Structure of Amantadine-Bound M2 Transmembrane Peptide of Influenza A in Lipid Bilayers from Magic-Angle-Spinning Solid-State NMR: The Role of Ser31 in Amantadine Binding. *J. Mol. Biol.* 385, 1127–1141.
- (24) Hong, M., Gross, J. D., Rienstra, C. M., Griffin, R. G., and Kumashiro, K. K.; et al. (1997) Coupling amplification in 2D MAS NMR and its application to torsion angle determination in peptides. *J. Magn. Reson.* 129, 85–92.
- (25) Cady, S. D., and Hong, M. (2008) Simultaneous extraction of multiple orientational constraints of membrane proteins by  $^{13}\text{C}$ -detected N-H dipolar couplings under magic angle spinning. *J. Magn. Reson.* 191, 219–225.
- (26) Hong, M., and Griffin, R. G. (1998) Resonance assignments for solid peptides by dipolar-mediated C-13/N-15 correlation solid-state NMR. *J. Am. Chem. Soc.* 120, 7113–7114.
- (27) Gullion, T., and Schaefer, J. (1989) Rotational-Echo Double-Resonance NMR. *J. Magn. Reson.* 81, 196–200.
- (28) Blough, H. A., and Merlie, J. P. (1970) Lipids of Incomplete Influenza Virus. *Virology* 40, 685–692.
- (29) Blough, H. A. (1971) Fatty Acid Composition of Individual Phospholipids of Influenza Virus. *J. Gen. Virol.* 12, 317–320.
- (30) Edidin, M. (2003) The State of Lipid Rafts: From Model Membranes to Cells. *Annu. Rev. Biophys. Biomol. Struct.* 32, 257–283.
- (31) Niemela, P. S., Hyvonen, M. T., and Vattulainen, I. (2009) Atom-scale molecular interactions in lipid raft mixtures. *Biochim. Biophys. Acta* 1788, 122–135.
- (32) Gambin, Y., Lopez-Esparza, R., Reffay, M., Sierceki, E., and Gov, N. S.; et al. (2006) Lateral mobility of proteins in lipid membranes revisited. *Proc. Natl. Acad. Sci. U.S.A.* 103, 2098–2102.
- (33) Lindblom, G., Oradd, G., and Filippov, A. (2006) Lipid lateral diffusion in bilayers with phosphatidylcholine, sphingomyelin and cholesterol: An NMR study of dynamics and lateral phase separation. *Chem. Phys. Lipids* 141, 179–184.
- (34) Jelinski, L. W., Sullivan, C. E., and Torchia, D. A. (1980)  $^2\text{H}$  NMR study of molecular motion in collagen fibrils. *Nature* 284, 531–534.
- (35) Jaroniec, C. P., Tounge, B. A., Rienstra, C. M., Herzfeld, J., and Griffin, R. G. (1999) Measurement of  $^{13}\text{C}$ - $^{15}\text{N}$  distances in uniformly  $^{13}\text{C}$  labeled biomolecules: J-decoupled REDOR. *J. Am. Chem. Soc.* 121, 10237–10238.
- (36) Pinto, L. H., Dieckmann, G. R., Gandhi, C. S., Papworth, C. G., and Braman, J.; et al. (1997) A functionally defined model for the M2 proton channel of influenza A virus suggests a mechanism for its ion selectivity. *Proc. Natl. Acad. Sci. U.S.A.* 94, 11301–11306.
- (37) Cady, S. D., and Hong, M. (2008) Amantadine-Induced Conformational and Dynamical Changes of the Influenza M2 Transmembrane Proton Channel. *Proc. Natl. Acad. Sci. U.S.A.* 105, 1483–1488.
- (38) Khurana, E., Dal Peraro, M., DeVane, R., Vemparala, S., and DeGrado, W. F.; et al. (2009) Molecular dynamics calculations suggest a conduction mechanism for the M2 proton channel from influenza A virus. *Proc. Natl. Acad. Sci. U.S.A.* 106, 1069–1074.
- (39) Cristian, L., Lear, J. D., and DeGrado, W. F. (2003) Use of thiol-disulfide equilibria to measure the energetics of assembly of transmembrane helices in phospholipid bilayers. *Proc. Natl. Acad. Sci. U.S.A.* 100, 14772–14777.
- (40) Schroeder, C., Heider, H., Möncke-Buchner, E., and Lin, T. I. (2005) The influenza virus ion channel and maturation cofactor M2 is a cholesterol-binding protein. *Eur. Biophys. J.* 34, 52–66.
- (41) Ma, C., Polishchuk, A. L., Ohigashi, Y., Stouffer, A. L., and Schön, A. (2009) Identification of the Functional Core of the Influenza A Virus A/M2 Proton-Selective Ion Channel. *Proc. Natl. Acad. Sci. U.S.A.* (in press).
- (42) Wang, J., Kim, S., Kovacs, F., and Cross, T. A. (2001) Structure of the transmembrane region of the M2 protein H<sup>+</sup> channel. *Protein Sci.* 10, 2241–2250.
- (43) Hu, J., Asbury, T., Achuthan, S., Li, C., and Bertram, R.; et al. (2007) Backbone structure of the amantadine-blocked transmembrane domain M2 proton channel from Influenza A virus. *Biophys. J.* 92, 4335–4343.
- (44) Duong-Ly, K. C., Nanda, V., DeGrado, W. F., and Howard, K. P. (2005) The conformation of the pore region of the M2 proton channel depends on lipid bilayer environment. *Protein Sci.* 14, 856–861.
- (45) Hu, J., Fu, R., Nishimura, K., Zhang, L., and Zhou, H.-X.; et al. (2006) Histidines, heart of the hydrogen ion channel from influenza A virus: Toward an understanding of conductance and proton selectivity. *Proc. Natl. Acad. Sci. U.S.A.* 103, 6865–6870.
- (46) Howard, K. P., Lear, J. D., and DeGrado, W. F. (2002) Sequence determinants of the energetics of folding of a transmembrane four-helix-bundle protein. *Proc. Natl. Acad. Sci. U.S.A.* 99, 8568–8572.
- (47) Salom, D., Hill, B. R., Lear, J. D., and DeGrado, W. F. (2000) pH-dependent tetramerization and amantadine binding of the transmembrane helix of M2 from the influenza A virus. *Biochemistry* 39, 14160–14170.
- (48) Luo, W., Mani, R., and Hong, M. (2007) Sidechain conformation and gating of the M2 transmembrane peptide proton channel of influenza A virus from solid-state NMR. *J. Phys. Chem.* 111, 10825–10832.
- (49) Luo, W., and Hong, M. (2006) Determination of the Oligomeric Number and Intermolecular Distances of Membrane Protein

- Assemblies by Anisotropic  $^1\text{H}$ -Driven Spin Diffusion NMR Spectroscopy. *J. Am. Chem. Soc.* 128, 7242–7451.
- (50) DeGrado, W. F., Gratkowski, H., and Lear, J. D. (2003) How do helix-helix interactions help determine the folds of membrane proteins? Perspectives from the study of homo-oligomeric helical bundles. *Protein Sci.* 12, 647–665.
- (51) Yang, J., Prorok, M., Castellino, F. J., and Weliky, D. P. (2004) Oligomeric  $\beta$ -structure of the membrane-bound HIV-1 fusion peptide formed from soluble monomers. *Biophys. J.* 87, 1951–1963.
- (52) Hiller, M., Krabben, L., Vinothkumar, K. R., Castellani, F., and van Rossum, B. J.; et al. (2005) Solid-state magic-angle spinning NMR of outer-membrane protein G from *Escherichia coli*. *ChemBioChem* 6, 1679–1684.
- (53) Schneider, R., Ader, C., Lange, A., Giller, K., and Hornig, S.; et al. (2008) Solid-state NMR spectroscopy applied to a chimeric potassium channel in lipid bilayers. *J. Am. Chem. Soc.* 130, 7427–7435.
- (54) Struts, A. V., Salgado, G. F., Tanaka, K., Krane, S., and Nakanishi, K.; et al. (2007) Structural analysis and dynamics of retinal chromophore in dark and meta I states of rhodopsin from  $^2\text{H}$  NMR of aligned membranes. *J. Mol. Biol.* 372, 50–66.
- (55) Lewis, B. A., Harbison, G. S., Herzfeld, J., and Griffin, R. G. (1985) NMR structural analysis of a membrane protein: Bacteriorhodopsin peptide backbone orientation and motion. *Biochemistry* 24, 4671–4679.
- (56) Kates, M., Kushwaha, S. C., and Sprott, G. D. (1982) Lipids of purple membrane from extreme halophiles and of methanogenic bacteria. *Methods Enzymol.* 88, 98–111.
- (57) Bunge, A., Muller, P., Stöckl, M., Herrmann, A., and Huster, D. (2008) Characterization of the ternary mixture of sphingomyelin, POPC, and cholesterol: Support for an inhomogeneous lipid distribution at high temperatures. *Biophys. J.* 94, 2680–2690.
- (58) Leser, G. P., and Lamb, R. A. (2005) Influenza virus assembly and budding in raft-derived microdomains: A quantitative analysis of the surface distribution of HA, NA and M2 proteins. *Virology* 342, 215–227.